Determination of Electromagnetic Phased-Array Driving Signals for Hyperthermia Based on a Steady-State Temperature Criterion

Marc E. Kowalski, *Student Member, IEEE,* and Jian-Ming Jin, *Senior Member, IEEE*

***Abstract*—Electromagnetic phased arrays can be used to preferentially heat tumors, potentially providing clinical benefit in oncological applications. Synthesizing a temperature field that exposes cancerous cells to sufficiently elevated temperatures while not harming healthy cells is not a trivial problem, and can often be assisted by the use of computational models of the patient. In this paper, a method for determining phased-array driving signals that result in a clinically favorable temperature distribution is presented. It is shown by example that simply focusing the power deposited over the tumor is not sufficient to guarantee that the peak temperature elevation occurs in the tumor in biological media. To remedy this, the temperature is predicted by a simple computational model and directly optimized as a function of the phased-array driving signals. To facilitate this optimization, superposition principles are used for both the electromagnetic and thermal models to minimize the number of computationally intensive forward problems that must be solved.**

***Index Terms*—Computational electromagnetics, hyperthermia, phased-array synthesis.**

I. Introduction

HYPERTHERMIA, or selective temperature elevation, can be used to treat cancerous tumors. It has been found that cancerous cells subjected to elevated temperatures are rendered more sensitive to chemical toxins and x-irradiation [1]. Hyperthermia can, therefore, be used to reduce the amount of conventional surgery, chemotherapy, and radiation necessary to treat cancer, reducing their associated undesirable side effects. In order to achieve these beneficial effects, a hyperthermia system must be able to preferentially heat the tumor, increasing the temperature in the majority of the tumor volume above 43 °C. In addition, the hyperthermia system should not raise the temperature of surrounding healthy tissue above 42 °C [2].

Electromagnetic radiation may be used to induce hyperthermia via ohmic heating of the tumor. A good deal of research over the past two decades has been conducted on the modeling of the electromagnetic and thermal aspects of RF hyperthermia. One of the problems for which the existing research has not yet provided a satisfactory solution is the focusing of electromagnetic radiation to preferentially heat "deep-seated" (located more than 7 cm below the surface of the skin) tumors. Focusing of energy through inhomogeneous patient tissue itself is a difficult problem since the specific inhomogeneities vary from patient to patient. Additionally, the amount of power that can be deposited in the tumor is frequently limited by the formation of undesired "hot spots" or auxiliary focal points, which can create patient discomfort.

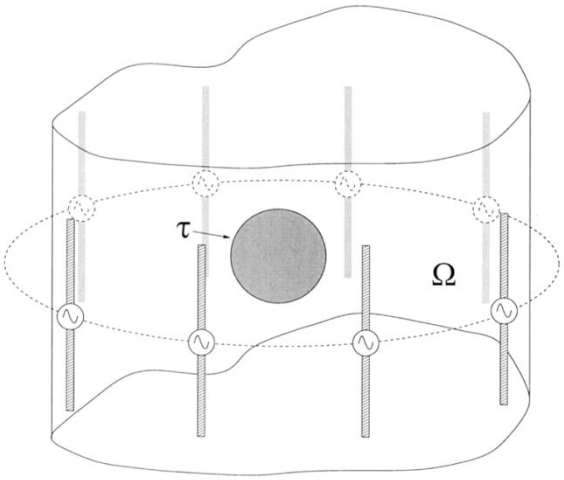

Fig. 1. Schematic representation of an APA of dipole antennae surrounding a patient volume (Ω) containing a tumor (τ). A water bolus usually fills the volume between the APA elements and patient.

Currently, the most popular approach for providing hyperthermia to deep-seated tumors noninvasively is to use an array of applicators placed around the periphery of the patient, allowing constructive wave interference to be exploited in heating the tumor. Devices designed on this principle are usually referred to as annular phased arrays (APAs) [3]. In an APA, the individual array elements are placed in a regular concentric pattern around the patient. Fig. 1 schematically depicts an APA of dipole antennae. A bolus filled with deionized water generally fills the space between the antennae and the patient to provide impedance matching and superficial cooling. The ability to choose the excitation amplitudes and phases of the elements of the array provides considerable flexibility in shaping the resultant power distribution pattern. However, the difficulty in noninvasively monitoring power deposition and temperature elevation together with the risk of damaging healthy tissue in a living patient mandate that the operator begin the treatment session with a set of parameters that preferentially heat the tumor. Due to inter-patient variability, even the most experienced operators do not have sufficient intuition to determine such a set of parameters before the treatment begins.

Manuscript received November 15, 1999; revised April 17, 2000. This work was supported by the National Science Foundation under a Graduate Fellowship and by the National Science Foundation under Grant NSF ECE 94-57735.

The authors are with the Department of Electrical and Computer Engineering, University of Illinois at Urbana-Champaign, Urbana, IL 61801 USA.

Publisher Item Identifier S 0018-9480(00)09537-5.

In response to this difficulty, a number of works have appeared which proposed systematic methods for determining phased-array driving signals in order to synthesize a favorably deposited power distribution. Two early pioneers in clinical applications of this type of procedure [4], [5] described in detail a procedure in which medical images (usually computed tomography (CT) images) of a specific patient are used to construct a computational electromagnetic model of the patient [6], [7]. The hyperthermia applicator to be used in the treatment session is then also incorporated into the model. Numerical optimization procedures could then be used to determine the driving phases and amplitudes of the array in order to optimally preferentially heat the tumor. Significant extensions and refinements of this idea have also been reported recently [8]–[10]. However, it is well known that the clinical effectiveness of a hyperthermia treatment depends on the temperature elevation achieved inside the tumor, not the power deposited. Complex thermodynamic effects, the most significant of which is blood flow, may render a promising power deposition distribution useless in terms of the resultant temperature elevation.

In order to overcome this difficulty, a number of researchers have proposed the direct optimization of the temperature field itself. The work presented in [11]–[13] suggested using temperature measurements along with a model-fitting procedure in order to find a linear state-space dynamical model of the hyperthermia process. Once this model is found, the resultant temperature field may be optimized in a straightforward manner. An alternative approach is presented in [2], [4], and [14]–[16], in which a detailed electromagnetic and thermal model of the patient is constructed based on medical images, and the optimization process is carried out on this computational representation of the patient. The advantage of the former approach is that feedback control may be used in order to continually monitor and adjust the treatment. The advantage of the latter approach is that it can incorporate *a priori* information about the patient and, therefore, eliminate the need for a *model-identification* stage of the treatment process, which may be intolerably long [11]. Additionally, the assumption of linear dynamics, which is typically necessary for model identification, is not rigorously justifiable for phased-array applicators.

In this paper, a method for the determination of APA driving signals is proposed, which makes use of a (possibly patient-specific) computational model of the APA and patient. Once such a model is obtained, a nonlinear optimization problem is formulated based on the requirement that the steady-state temperature field be clinically beneficial. This optimization problem is then solved numerically in conjunction with the computational model. This procedure may be used to determine a set of driving parameters to provide acceptable hyperthermia without exposing the patient to the risks of tuning the parameters once the treatment has begun. Additionally, the same patient model may be used with several different applicators in order to determine the relative merits of each applicator.

The finite-difference time-domain (FDTD) [17] method is used in this work to numerically model the electromagnetics of the hyperthermia applicator and patient. The use of the FDTD in hyperthermia treatment planning has been widely reported [18]–[21] and validation of the predictions made by the FDTD in this context has been performed [22]. Since the FDTD has modest computational requirements, a full three-dimensional model of the patient and applicators can easily be simulated. This is in contrast to the volume-surface integral-equation (VSIE) technique used in [2], which required that the water bolus of the applicator be approximated as an homogeneous background medium to ease computational requirements. It has recently been shown that surface-wave phenomena along the bolus–air interface may play a significant role in the behavior of the APA [23] and can be captured by the FDTD. It should also be noted that, as in [9], it is possible to model the effects of array element coupling in the FDTD.

Finite differences are also used in this work to numerically model the steady-state bio-heat transfer equation (BHTE) [24]. The limitations of the BHTE are well known, but for the relatively large tumors, which are candidates for deep RF hyperthermia, its ability to predict temperature elevations is still useful. The BHTE has been used and validated to some extent previously in the modeling of electromagnetic hyperthermia devices [25], [26]. Numerical solution of the BHTE provides the capability to model arbitrary three-dimensional inhomogeneities in thermal constitutive parameters of the patient. This is in contrast to the approach used in [14], in which a detailed three-dimensional model of the electromagnetics was used in conjunction with the half-space Green's function solution of the BHTE. Such a thermal model is necessarily approximate and wastes information about tissue inhomogeneity obtained in the formation of the patient-specific electromagnetic tissue model.

Special emphasis is placed in this paper on the efficient optimization of the temperature field. To achieve an efficient optimization, a superposition principle is introduced similar to that recently proposed in other works [15], [16]. However, unlike the Monte Carlo search procedure used in [15], this work employs a gradient-descent scheme to optimize the temperature field. To facilitate the efficient evaluation of both the objective function and its gradient, this paper provides the extension suggested in [16] of the superposition principle to the evaluation of partial derivatives of the temperature field with respect to the phased-array driving signals.

This paper provides a detailed account of the formulation and implementation of the proposed method along with illustrative numerical examples of its use. Section II motivates the use of an optimization criterion and describes the efficient numerical determination of optimal driving parameters. Section III provides examples of the use of the method using an anatomically detailed two-dimensional patient model. An example is provided in which the point of peak temperature elevation does not coincide with the point of peak power absorption, evidencing the need for direct optimization of the temperature field. A three-dimensional example involving a muscle-equivalent phantom is included to illustrate the efficiency of the method when applied to computationally intensive three-dimensional models. Section IV discusses possible refinements of the method, including the use of alternate thermal models and various numerical methods for modeling and optimization.

II. Method

In this section, the details of the proposed method are presented. Motivation is provided for the formulation of an optimization problem whose solution corresponds (when possible) to an idealized temperature field. An electromagnetic and thermal superposition principle is introduced to reduce the computational cost of numerically performing the optimization.

A. Formulation of an Optimality Criterion

Let Ω denote the volume of the body of the patient and τ denote the volume of the tumor, as depicted in Fig. 1. A reasonable goal for hyperthermic treatment of the tumor is to find a set of APA driving parameters such that the resultant steady-state temperature field $T(\boldsymbol{r})$ satisfies the following inequalities:

$$\begin{aligned} T(\boldsymbol{r}) &\geq T_1, \qquad \boldsymbol{r} \in \tau \\ T(\boldsymbol{r}) &\leq T_2, \qquad \boldsymbol{r} \in \Omega \backslash \tau \end{aligned} \tag{1}$$

where T_1 is the minimal desired temperature in the tumor and T_2 is the maximum temperature allowed in healthy tissue. In this way, temperature elevations high enough to facilitate cytotoxia are experienced only in the tumor.

As a practical matter, the above specifications (1) are enforced only at a finite number of points

$$\begin{aligned} T(\boldsymbol{r}_p^t) &\geq T_1, \qquad \text{for } p = 1, 2, \ldots, P \\ T(\boldsymbol{r}_q^h) &\leq T_2, \qquad \text{for } q = 1, 2, \ldots, Q \end{aligned} \tag{2}$$

where $\boldsymbol{r}_p^t \in \tau$ are points inside the tumor volume and $\boldsymbol{r}_q^h \in \Omega \backslash \tau$ are points inside healthy tissue. However, even with the less stringent requirement that the inequalities be met at a discrete number of points, the possibility exists that no set of driving parameters can be found that satisfies (2).

As an alternative, consider the goal of the minimization of the performance index

$$J(\boldsymbol{u}) = \frac{1}{P} \sum_{p=1}^{P} \left[\min \left\{ T(\boldsymbol{r}_p^t) - T_1, 0 \right\} \right]^2 + \frac{\mu}{Q} \sum_{q=1}^{Q} \left[\min \left\{ T_2 - T(\boldsymbol{r}_q^h), 0 \right\} \right]^2 \tag{3}$$

where $\boldsymbol{u}$ is a vector representing the set of array driving parameters (which will be defined more precisely in Section II-B) and μ is a free parameter used to adjust the relative importance of heating the tumor and protecting healthy tissue. It is clear that the minimal value $J = 0$ is achieved if and only if (2) is exactly satisfied. Additionally, it should be clear that increased values of J correspond to more serious violations of (2).

The adoption of the minimization of (3) as the goal of the procedure has in essence accomplished two things. First, minimization of J implies that the inequalities (2) are enforced "softly," i.e., that they are met as closely as possible. In fact, the function J can be interpreted as a penalty function [27], which frequently appears in the conversion of constrained optimization problems into unconstrained problems. Secondly, the minimization of J can be accomplished systematically by taking an initial set of driving parameters for which $J \neq 0$ and using an unconstrained search procedure in order to try to achieve $J = 0$, whereas no systematic approach is immediately apparent for trying to achieve (2) directly.

In summary, it is desired to find a set of APA driving parameters that satisfy

$$\boldsymbol{u}^* = \arg\min J(\boldsymbol{u}) \tag{4}$$

where the performance index $J(\boldsymbol{u})$ is as defined in (3). In the above, $\boldsymbol{u}^*$ is any vector (not necessarily unique) that achieves the minimum of J.

B. Numerical Modeling and Optimization

In order to solve the optimization problem (4) without actually applying many different driving signals to an array and measuring the result on a patient, it is necessary to have a model that can predict the steady-state temperature field resulting from a given input. In this paper, this is accomplished by the numerical FDTD [17] model of the electromagnetics and a finite-difference–BHTE (FD–BHTE) model [28]. Together these two techniques give the capability to predict the steady-state temperature field due to a given array excitation.

The state of the APA may be defined by the real and imaginary parts of each of the N excitations. These can be lumped together into a $2N$ vector

$$\boldsymbol{u} = \left(u_r^{(1)}, u_i^{(1)}, \ldots, u_r^{(N)}, u_i^{(N)} \right) \tag{5}$$

where the notation $u_r^{(l)}$ and $u_i^{(l)}$ refer to the *real* and *imaginary* parts of the driving signal of the lth element of the array, respectively. Note that it is only necessary to use $2N-1$ parameters to characterize the array, e.g., the N amplitudes and $N-1$ relative phases. Definition (5) adds one unnecessary dimension to the state of the applicator. However, this will serve to considerably simplify notation in the developments that follow. In this formulation, it is immediately clear that the excitation parameters need not be restricted in any way. Additionally, the use of the real and imaginary parts instead of the amplitudes and phases of the driving signals (as in [14] and [16]) has been found through experience to render the optimization problem better conditioned numerically.

A naive way to begin the minimization of (3) would be to use the FDTD and FD-BHTE models and directly compute the temperature distributions and estimate the gradients in the course of a numerical search procedure. However, due to the considerable expense of resolving the electromagnetic [5] and thermal models [4], an alternative method is pursued here which minimizes the number of uses of the FDTD and FD–BHTE numerical procedures.

Since the electromagnetic field is linear in terms of individual element excitations, it may be computed as

$$\boldsymbol{E}(\boldsymbol{r}) = \sum_{l=1}^{N} \left(u_r^{(l)} + j u_i^{(l)} \right) \boldsymbol{E}^{(l)}(\boldsymbol{r}) \tag{6}$$

where $\boldsymbol{E}^{(l)}(\boldsymbol{r})$ is the electric field produced by unitary excitation of the lth element of the array in solitude.

In a similar way, the total specific absorption rate (SAR), or time-average power deposited per unit mass of tissue, can be computed

$$\mathrm{SAR}(\boldsymbol{r}) = \frac{\sigma(\boldsymbol{r})}{2\rho(\boldsymbol{r})}\left|\sum_{l=1}^{N}\left(u_r^{(l)} + ju_i^{(l)}\right)\boldsymbol{E}^{(l)}(\boldsymbol{r})\right|^2. \quad (7)$$

It is convenient at this point to define the cross correlation of the electric fields due to the lth and kth array elements

$$\Xi_{lk}(\boldsymbol{r}) = \boldsymbol{E}^{(l)^\dagger}(\boldsymbol{r})\boldsymbol{E}^{(k)}(\boldsymbol{r}) \quad (8)$$

where † denotes conjugate transposition. Notice that this is a complex-valued scalar whose value varies with position inside the patient. It will be apparent later that it is advantageous to express the SAR in terms of the cross correlation

$$\mathrm{SAR}(\boldsymbol{r}) = \frac{\sigma(\boldsymbol{r})}{2\rho(\boldsymbol{r})}\sum_{l=1}^{N}\sum_{k=1}^{N}\left(u_r^{(l)} - ju_i^{(l)}\right)\left(u_r^{(k)} + ju_i^{(k)}\right)\Xi_{lk}(\boldsymbol{r}). \quad (9)$$

In order to predict the steady-state temperatures once the SAR field is known, it is necessary to have some type of thermal model. One of the simplest thermal models that can adequately describe the evolution of temperature in biological media is the BHTE [24] due to Pennes. The steady-state form of the BHTE is given by

$$\nabla\cdot k(\boldsymbol{r})\nabla T(\boldsymbol{r}) + v_b(\boldsymbol{r})\big(T_a - T(\boldsymbol{r})\big) + \rho(\boldsymbol{r})\mathrm{SAR}(\boldsymbol{r}) = 0 \quad (10)$$

where k ($\mathrm{Wm^{-1}K^{-1}}$) is the local thermal conductivity, v_b ($\mathrm{Wm^{-3}K^{-1}}$) is the product of the specific heat of blood and its local mass flow rate per unit volume, and T_a (K) is the arterial blood temperature. The effect of metabolic heat generation has been neglected since the heat generated by hyperthermia applicators is typically an order of magnitude greater than this.

Equation (10) requires a set of boundary conditions in order to have a well-defined solution. Typically, a convective boundary condition is imposed at the tissue–bolus interface and a Dirichlet (fixed-temperature) boundary condition is imposed on the axial-plane surfaces where the patient model is artificially truncated. In this paper, only inhomogeneous Dirichlet boundary conditions are used for simplicity (as in [15])

$$T(\boldsymbol{r})|_{\mathrm{boundary}} = T_b(\boldsymbol{r}) \quad (11)$$

where the boundary is taken as union of the tissue–bolus interface and the surfaces at which the human model is artificially truncated. It is assumed that the temperature of the tissue–bolus interface is fixed at 10 °C, and that of the body (used at the artificial truncation boundary) is fixed at 37 °C.

No matter what type of boundary conditions are assumed, the differential operator in (10) can be approximated by finite differences, yielding (together with the boundary conditions) a linear system for the temperature at a discrete set of points

$$\overline{\boldsymbol{A}}\boldsymbol{T} = \boldsymbol{b}(\boldsymbol{u}) + \boldsymbol{d}. \quad (12)$$

In the above expression, $\boldsymbol{T}$ is an M vector of temperatures at M distinct points in space, $\boldsymbol{b}(\boldsymbol{u})$ is a vector related to the local heat deposited, which depends on the input, $\boldsymbol{d}$ is a forcing term related to perfusion and boundary conditions, and $\overline{\boldsymbol{A}}$ is an $M \times M$ matrix generated from the finite-difference approximation of the differential operator. For Dirichlet boundary conditions, the mth element of each of these vectors may be expressed as

$$T_m = T(\boldsymbol{r}_m) \quad (13)$$

$$b_m(\boldsymbol{u}) = (1 - d(m))\,\rho(\boldsymbol{r}_m)\mathrm{SAR}(\boldsymbol{r}_m) \quad (14)$$

$$d_m = (1 - d(m))\,v_b(\boldsymbol{r}_2)T_a + d(m)T(\boldsymbol{r}_m) \quad (15)$$

where $d(m)$ is equal to one if the point $\boldsymbol{r}_m$ is on the boundary and zero if it is not. When the point $\boldsymbol{r}_m$ is on the boundary, the mth row and column of $\overline{\boldsymbol{A}}$ are empty, except for a unit diagonal element. Otherwise, the matrix consists of entries related to the finite-difference approximation of the differential operator [28], [32].

At first glance, it would seem that the system (12) needs to be solved each time any component of the input vector is changed. This could quickly lead to a computational bottleneck in an optimization procedure [4], because many temperature field evaluations are typically necessary in the course of a numerical search procedure. However, closer examination of (12) reveals two important facts. Firstly, the vector $\boldsymbol{d}$ does not depend on the input, thus, the temperature vector $\boldsymbol{T}_d = \overline{\boldsymbol{A}}^{-1}\boldsymbol{d}$ can be computed once and stored. Secondly, the definition of the vector $\boldsymbol{b}$ together with the compact expression (9) for computing the SAR at any point reveals that any element of $\boldsymbol{b}$ may be expressed

$$b_m = \frac{\sigma(\boldsymbol{r}_m)}{2}\sum_{l=1}^{N}\sum_{k=1}^{N}\left(u_r^{(l)} - ju_i^{(l)}\right)\left(u_r^{(k)} + ju_i^{(k)}\right)\Xi_{lk}(\boldsymbol{r}_m). \quad (16)$$

This, in turn, implies that the vector $\boldsymbol{b}$ can be expressed

$$\boldsymbol{b} = \frac{1}{2}\sum_{l=1}^{N}\sum_{k=1}^{N}\left(u_r^{(l)} - ju_i^{(l)}\right)\left(u_r^{(k)} + ju_i^{(k)}\right)\boldsymbol{B}_{lk} \quad (17)$$

where a set of weighted correlation "basis" vectors $\boldsymbol{B}_{lk}$ have implicitly been defined, which have $(1 - d(m))\sigma(\boldsymbol{r}_m)\Xi_{lk}(\boldsymbol{r}_m)$ as their mth element. If the N^2 basis vectors are formed and the temperature distribution due to each of them ($\boldsymbol{T}_{lk} = \overline{\boldsymbol{A}}^{-1}\boldsymbol{B}_{lk}$) is found and stored, then the temperature due to an arbitrary set of excitation parameters can be readily calculated as follows:

$$\boldsymbol{T} = \boldsymbol{T}_d + \frac{1}{2}\sum_{l=1}^{N}\sum_{k=1}^{N}\left(u_r^{(l)} - ju_i^{(l)}\right)\left(u_r^{(k)} + ju_i^{(k)}\right)\boldsymbol{T}_{lk}. \quad (18)$$

When using gradient-based search procedures to numerically minimize (3), it is also necessary to repeatedly compute partial derivatives with respect to the excitation parameters. These can be computed from the following formula:

$$\nabla_{\boldsymbol{u}}J(\boldsymbol{u}) = \frac{1}{P}\sum_{p=1}^{P}\begin{cases}0, & \text{if } T(\boldsymbol{r}_p^t) \geq T_1\\ 2[T(\boldsymbol{r}_p^t) - T_1]\nabla_{\boldsymbol{u}}T(\boldsymbol{r}_p^t), & \text{else}\end{cases} + \frac{\mu}{Q}\sum_{q=1}^{Q}\begin{cases}0, & \text{if } T(\boldsymbol{r}_q^h \leq T_2\\ 2[T(\boldsymbol{r}_q^h) - T_2]\nabla_{\boldsymbol{u}}T(\boldsymbol{r}_q^h), & \text{else.}\end{cases} \quad (19)$$

The evaluation of the gradients in the above expression can be accomplished in an efficient manner by manipulating (18) to arrive at

$$\frac{\partial}{\partial u_r^{(m)}} T(\boldsymbol{r}_i) = \sum_{k=1}^{N} \left[u_r^{(k)} \Re\left\{ \boldsymbol{c}^T \boldsymbol{T}_{mk} \right\} - u_i^{(k)} \Im\left\{ \boldsymbol{c}^T \boldsymbol{T}_{mk} \right\} \right] \tag{20}$$

$$\frac{\partial}{\partial u_i^{(m)}} T(\boldsymbol{r}_i) = \sum_{k=1}^{N} \left[u_i^{(k)} \Re\left\{ \boldsymbol{c}^T \boldsymbol{T}_{mk} \right\} + u_r^{(k)} \Im\left\{ \boldsymbol{c}^T \boldsymbol{T}_{mk} \right\} \right] \tag{21}$$

where $\Re\{\cdot\}$ and $\Im\{\cdot\}$ denote the real and imaginary parts of their arguments, respectively, and $\boldsymbol{c}$ is a vector consisting of all zeros, except for one in the position corresponding to $\boldsymbol{r}_i$. It is assumed that the discrete positions ($\boldsymbol{r}_p^t$, $\boldsymbol{r}_q^h$) involved in the computation of the performance index coincide with points at which the temperature field is known from the FD-BHTE ($\boldsymbol{r}_i$).

The evaluation of the performance index and its gradient requires the one-time cost of evaluating the N^2 basis vectors. It then costs very little to compute gradients and function values *on the fly*. In a naive implementation, where the FDTD and FD-BHTE are continually used to compute function values and gradients as the driving signals are changed, each iteration of a search procedure would be considerably more expensive. In practice, for detailed three-dimensional computational models, the number of unknowns required for detailed modeling makes this a considerable hindrance to optimization.

In summary, the proposed procedure is: 1) use the FDTD to compute the electric fields $\boldsymbol{E}^{(l)}(\boldsymbol{r})$ due to each of the N independent array elements; 2) compute $\boldsymbol{T}_d = \overline{\boldsymbol{A}}^{-1}\boldsymbol{d}$ using the FD-BHTE; 3) form the N^2 basis vectors $\boldsymbol{B}_{lk}$ and compute the N^2 quantities $\boldsymbol{T}_{lk} = \overline{\boldsymbol{A}}^{-1}\boldsymbol{B}_{lk}$; and 4) begin a numerical search procedure to minimize J. In this paper, the Fletcher–Reeves variant of the conjugate-gradient (CG) method of unconstrained nonlinear optimization, as described in [27], is used to try to drive the performance index to zero.

III. Numerical Examples

In this section, two numerical examples of application of the method are presented. The first example employs an anatomically realistic model of a human trunk to illustrate the ability of the method to deal with inhomogeneities in the patient model and the importance of thermal inhomogeneities in treatment planning. The second example employs a three-dimensional model of a tissue-like phantom designed by the Center for Devices and Radiological Health (CDRH) Division, United States Food and Drug Administration (FDA). The discretization of the three-dimensional model leads to a computationally intensive optimization problem. It is shown that the method proposed in this paper is considerably more efficient than a naive optimization in this case.

A. Two-Dimensional Analysis of a Realistic Human Trunk

In this section, examples of the optimization technique are considered that involve two-dimensional anatomically realistic models of the human trunk region. When conditions of strong axial symmetry exist, two-dimensional models, although approximate, can provide valuable insight. In the axial midplane of a patient surrounded by an APA of z-directed dipoles, some axial symmetry does exist.

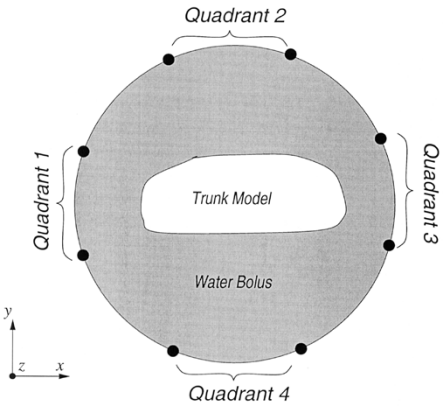

Fig. 2. Two-dimensional model of an APA and human trunk. The APA has four independent elements (quadrants), each composed of two dipoles.

Fig. 2 depicts the axial midplane of the APA enclosing a water bolus and the human trunk. The radius of the APA is taken to be 30 cm, which corresponds to that of a commercially available device [23]. The elements of the APA are dipoles, which are modeled in the two-dimensional FDTD by z-directed line current sources. Each independent element of the array is composed of two adjacent dipoles, leading to four independent quadrants.

Fig. 3 depicts two anatomically realistic models, which have been obtained based on the segmented human model presented in [30]. Each model is composed of six distinct tissue types: bone, colon, fat, muscle, spinal nerve, and tumor. The spatial resolution of these models is 8 mm^2, which is also the spatial resolution used for both the FDTD and FD-BHTE models. The temperature at the tissue–bolus interface was assumed to be 10 °C, which corresponds to the case when the deionized water in the bolus is used for cooling the patient. The electromagnetic operating frequency was chosen to be 85 MHz, which is within the operating range of available devices and avoids possible resonances in the FDTD model recently reported [23]. The computational domain of the FDTD is truncated by five cells of the perfectly matched layer (PML) [31] in each direction. For further details of the numerical modeling used, the reader is referred to [32].

In each model, a circular tumor of radius 2 cm has been placed. The position of the tumor is not meant to mimic any specific type of cancer. The two tumor locations were chosen for the challenge they pose to achieving acceptable temperature distributions. In the first model [Fig. 3(a)], the tumor is in the immediate vicinity of unperfused tissues, which creates difficulty in achieving a favorable temperature distribution in the tumor even if the SAR can be focused there. In the second model [Fig. 3(b)], the tumor is offset 10 cm away from the center of the APA, requiring careful phase and amplitude selection to focus the SAR in the appropriate position. The electromagnetic and thermal properties of the various tissue types used in the simulations in this paper are summarized in Table I and have been adapted from [33]–[35].

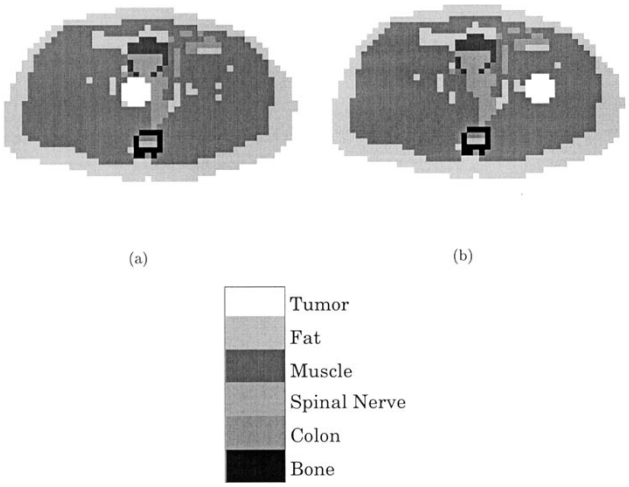

Fig. 3. Realistic tissue models of the human trunk used in the two-dimensional modeling. (a) Central tumor. (b) Tumor offset 10 cm from center.

TABLE I
ELECTRICAL AND THERMAL PROPERTIES OF TISSUES AT 85 MHz

Tissue Type	k ($\mathrm{Wm^{-1}K^{-1}}$)	v_b ($\mathrm{kWm^{-3}K^{-1}}$)	ϵ_r	σ ($\Omega^{-1}\mathrm{m}^{-1}$)
Tumor	0.50	1.25	80	0.72
Tumor (well-perfused)	0.50	3.33	80	0.72
Muscle	0.50	5.50	68	0.72
Spinal Nerve	0.52	0	50	0.33
Fat	0.23	0	13	0.07
Colon	0.56	0	86	0.66
Bone	1.47	0	15	0.15

Fig. 4 shows the result of uniform phase and amplitude ($\boldsymbol{u} = \{1, 1, 1, 1, 1, 1, 1, 1\}^T/\sqrt{2}$) excitation of the array. (All vectors reported in this section have been normalized such that $|u_r^{(1)} + ju_i^{(1)}| = 1$. The overall power level is left as a degree of freedom for the optimization, but the nature of the two-dimensional approximation makes it difficult to estimate the true power level needed in practice.) The tumor is located in the center of the array, thus, this is the most intuitive excitation to use, and it is clear from Fig. 4 that the SAR is indeed focused on the tumor. It is evident, however, that the unperfused colon and bone tissues experience the highest temperature elevations.

Fig. 5 shows the result obtained when the optimization technique described in this paper is used. Here, the parameters for optimization used were $T_1 = 44$ °C, $T_2 = 41$ °C, $\mu = 0.02$, $P = 45$, and $Q = 1140$. All of the points available from the FD-BHTE have been incorporated into the computation of the performance index, resulting in large values of P and Q. It is noted that in this case $Q/P \approx \mu$, so that approximately equal weight is given to any violation inside the tumor and any violation in the healthy tissue. The optimal relative driving signals obtained were $\boldsymbol{u} = \{0.1964, 0.9805, 0.0536, 1.7888, 1.8212, 1.6693, 1.5596, 0.6599\}^T$. It is seen from Fig. 5 that although the result does not heat the tumor completely uniformly and heats some of the healthy tissue to above $T_2 = 41$ °C, the result is certainly much more acceptable than the unoptimized result of Fig. 4. This is a case where, due to the

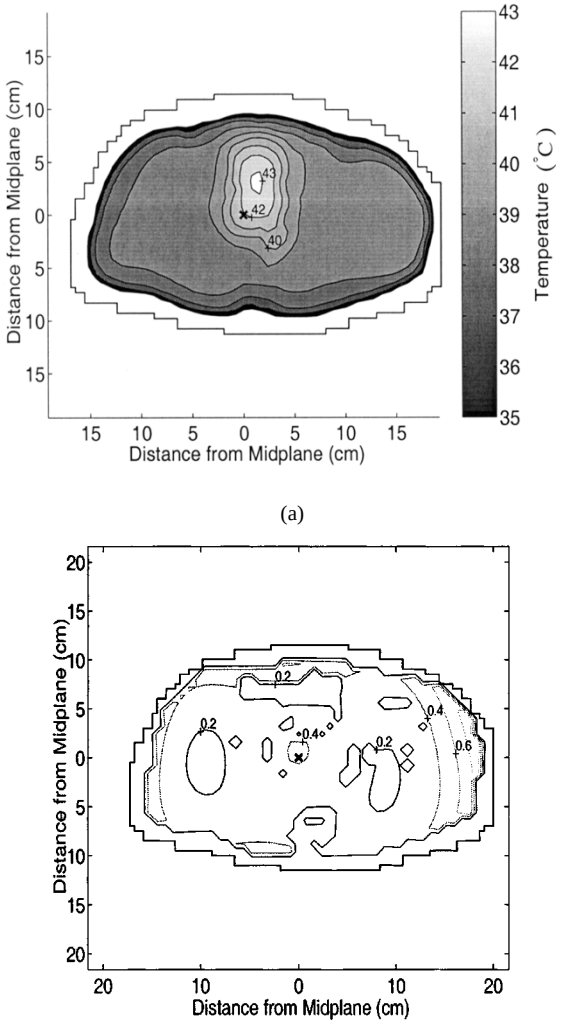

Fig. 4. Result for equal phase and amplitude driving of the APA on all four quadrants. The center of the 2-cm-radius tumor is indicated by a cross (×). The operating frequency is 85 MHz. The tissue–bolus interface is indicated by a solid line. (a) Steady-state temperature. (b) SAR.

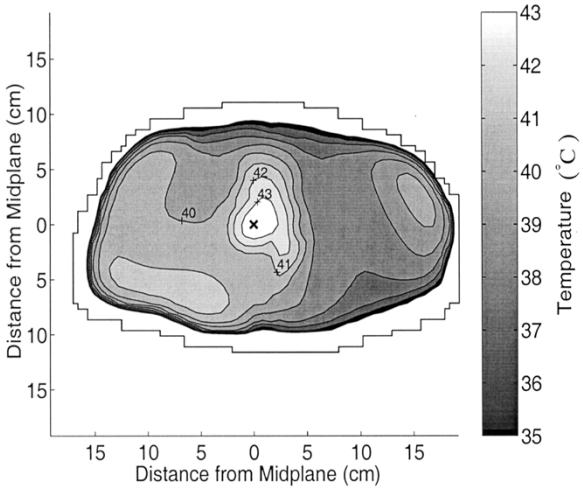

Fig. 5. Temperature field resulting from optimized driving signals for centrally located tumor. The center of the 2-cm-radius tumor is indicated by a cross (×) and the tissue–bolus interface is indicated by a solid line.

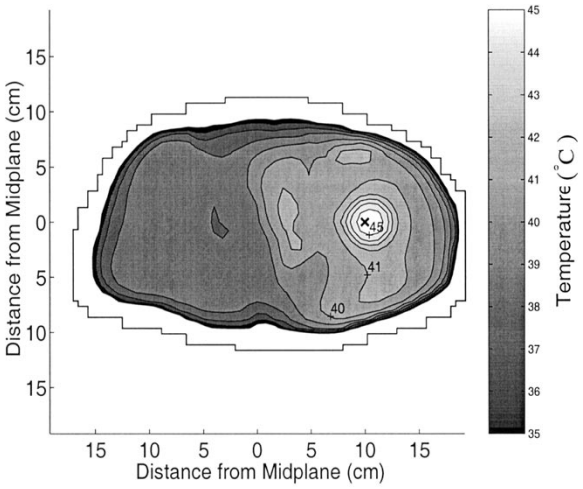

Fig. 6. Temperature field resulting from optimized driving signals for tumor offset 10 cm along the major axis of the patient. The center of the 2-cm-radius tumor is indicated by a cross ($\times$) and the tissue–bolus interface is indicated by a solid line.

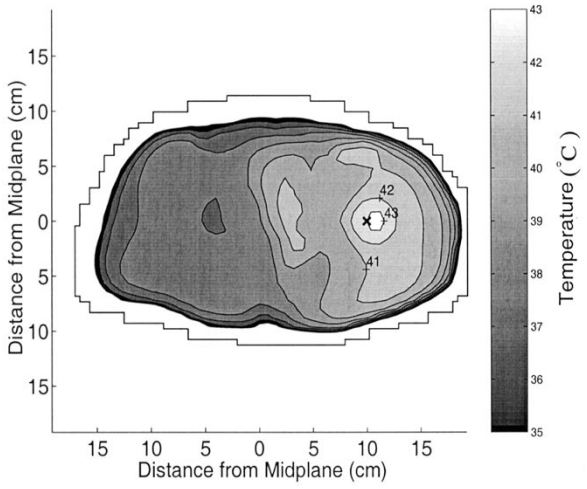

Fig. 7. Temperature field resulting from optimized driving signals for a well-perfused tumor offset 10 cm along the major axis of the patient. The center of the 2-cm-radius tumor is indicated by a cross ($\times$) and the tissue–bolus interface is indicated by a solid line.

inhomogeneity in perfusion rates, detailed thermal modeling is essential to obtaining an acceptable solution.

Next, the preferential heating of the tumor offset 10 cm from the center of the trunk, as depicted in Fig. 3(b), is considered. Fig. 6 depicts the optimal result obtained in this case, where the parameters for the optimization have been selected as in the previous example. It is clear that a strong focus in the temperature field is possible in this case, generating a desirable result. It should be noted that, in this case, the tumor is surrounded by muscle, which has similar thermal constitutive parameters. The optimal relative excitation vector obtained was $\boldsymbol{u} = \{0.9998, 0.0183, 0.0244, 0.5429, -1.1243, 0.1705, 0.1528, 0.8187\}^T$.

Fig. 7 shows the optimal result obtained when attempting to heat the same tumor, but with the tumor assumed to be much more well perfused ($v_b = 3300$ Wm^{-3}K^{-1}). It can be seen that, although a focus is still obtainable in the temperature field, it is more diffuse since the perfusion tends to remove heat away from regions of elevated temperature. The optimal relative excitation vector obtained was $\boldsymbol{u} = \{0.9972, -0.0753, 0.0960, 0.6072, -1.1098, 0.2138, 0.2390, 0.8930\}^T$, which is, as expected, quite similar to the one obtained in the last example.

B. Three-Dimensional Analysis of a Phantom

In this section, results of application of the proposed method to a three-dimensional model of the CDRH phantom are presented. Fig. 8 depicts the CDRH phantom, which is an elliptical cylinder, 57 cm in length, with major and minor axes of 32 and 22 cm, respectively [23]. It is mostly composed of muscle, with a thin superficial fat layer 1 cm in thickness around its circumference. Once again, spherical tumors 2 cm in radius have been placed in various positions in the phantom. It is noted that, in the results of this section, the tumors have been assumed to be well perfused exclusively since the homogeneous background (muscle) of the tumor makes achieving a focus in the temperature field considerably easier than in the case where the background is heavily inhomogeneous.

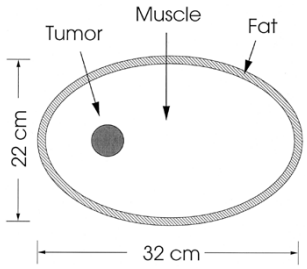

Fig. 8. Cross section of the 57-cm-long CDRH phantom.

The APA considered here is the same as that in the two-dimensional modeling. The dipoles are 44 cm in length and are modeled simply as z-directed current sources with a sinusoidal z dependence in the FDTD. Again, the RF operating frequency was chosen to be 85 MHz. The thermal boundary conditions assumed were $T = 10$ °C at the tissue–water interface, $T = 25$ °C at the tissue–air interface, and $T = 37$ °C at the upper and lower surfaces of the phantom.

In the three-dimensional case, the number of unknowns in the thermal model rises from 1185 for the two-dimensional model to 39 584. If detailed highly accurate temperature information is required, this number could be even larger. Table II evidences the savings in computation time made possible by precomputing the 16 basis temperatures and superposing them via (18), (20), and (21) to evaluate the objective function and its gradients (referred to as the superposition method in the table) rather than resolving the FD-BHTE system for each function and gradient evaluation (referred to as the direct method in the table). In practice, it was found that for a relative functional tolerance of 10^{-3}, 10–20 iterations of the CG are needed for convergence of the optimization problem. The line minimization in the nonlinear CG method requires about five function evaluations per iteration. This implies that 50–100 function evaluations and 10–20 gradient evaluations were needed in the course of a typical op-

TABLE II
AVERAGE CPU TIME REQUIRED ON A 500-MHz DEC ALPHA FOR ONE FUNCTION AND GRADIENT EVALUATION

Model	Unknowns	Method of Function Evaluation		Method of Gradient Evaluation	
		Direct Method	Superposition	Direct Method	Superposition
2D	1185	0.10 s	0.04 s	0.57 s	0.05 s
3D	39534	1.53 s	0.69 s	10.38 s	0.65 s

timization. The CPU times in Table II (for a 500-MHz DEC Alpha) show that the time to compute the objective function is reduced by a factor of approximately two and the time to compute the objective function's gradient is reduced by a factor of approximately ten when the superpositioning technique is used. Considering the large number of function and gradient evaluations needed, this leads to a considerable savings in computation time when the superposition method is employed.

Fig. 9 shows the temperature distribution obtained when the tumor is located centrally in the phantom. Here, the parameters for the optimization used were $T_1 = 44\,^{\circ}\mathrm{C}$, $T_2 = 41\,^{\circ}\mathrm{C}$, $\mu = 0.4$, $P = 13$, and $Q = 586$. All of the points available from the FD-BHTE in the axial midplane have been incorporated into the computation of the performance index. The optimal relative driving signals obtained were $\boldsymbol{u} = \{0.7099, 0.7043, 0.7370, 0.7425, 0.6539, 0.6629, 0.7058, 0.6953\}^T$. The estimated powers delivered to each quadrant in this case were 46.7, 48.5, 45.3, and 46.3 W for quadrants 1–4, respectively.

Fig. 10 shows the temperature distribution obtained when the tumor is offset 10 cm along the major axis of the phantom. The parameters for optimization used were the same as the previous example. The optimal relative driving signals obtained were $\boldsymbol{u} = \{0.6765, 0.7364, 0.0411, 0.3292, 0.6377, 0.7165, 0.4326, 0.2989\}^T$. The estimated powers delivered to each quadrant in this case were 32.4, 15.6, 21.3, and 15.9 W for quadrants 1–4, respectively.

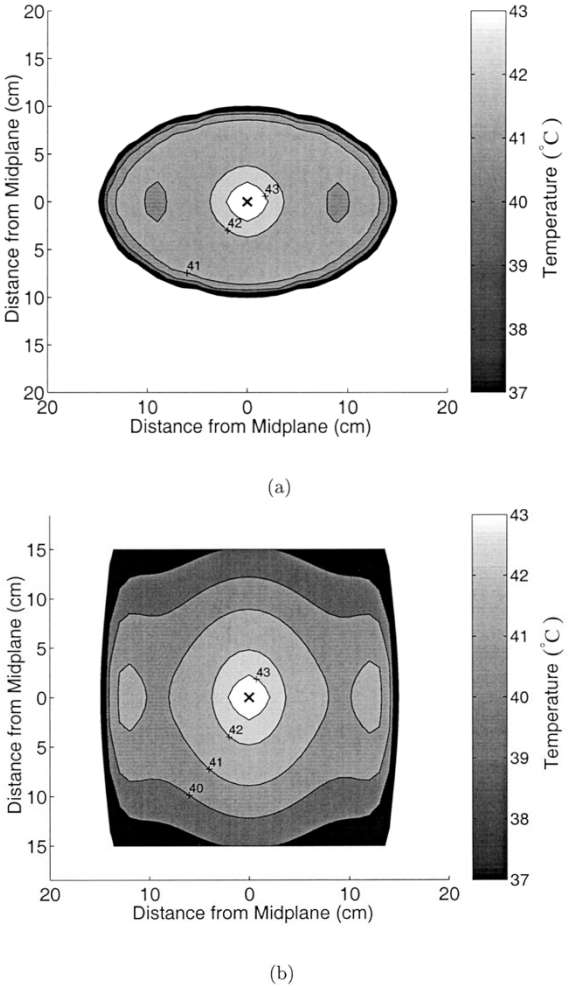

Fig. 9. Temperature field resulting from optimized driving signals for a well-perfused tumor embedded in the CDRH phantom. The center of the 2-cm-radius tumor is indicated by a cross (×). (a) Axial midplane. (b) Coronal midplane.

IV. EXTENSIONS

It should be noted that the gradient-based search procedure used in this paper is not a robust global optimizer. Many superior techniques, especially combinatorial ones such as genetic algorithm and simulated annealing, exist for finding true global extrema in nonconvex optimization problems. The technique proposed in this paper can still be used, however, to accelerate the many function evaluations required in these techniques.

Nikita *et al.* [14] and Lang *et al.* [16] have both used stabilized Newton-type techniques successfully for steady-state temperature optimization. Expressions for the Hessian similar to (19), (20), and (21) can also be derived in terms of the N^2 basis temperature vectors. It is, therefore, also possible to accelerate a Newton-type optimization scheme using the techniques proposed in this paper.

Note that the ability to find explicit expressions for the value and gradient of the objective function relies on only two essential features of the underlying physical models. First, the electromagnetic field must depend *linearly* on the excitation parameters. This is generally the case, even when aperture applicators are used. Secondly, the steady-state temperature field must depend *linearly* on the SAR, implying a kind of "quadratic" dependence on the excitation parameters. If these two requirements are met, the temperature field can be decomposed into a sum of temperature fields due to each independent element of the cross correlation of the electric fields. Convective boundary conditions and alternative thermal models to the BHTE may, therefore, be used in conjunction with the techniques of this paper to provide enhanced efficiency in temperature field optimization.

V. CONCLUSIONS

A simple and efficient method has been presented for synthesizing steady-state temperature fields that satisfy clinical requirements for hyperthermia. Electromagnetic and thermal models, which can incorporate arbitrary inhomogeneities, have been used to predict steady-state temperature fields. The goal of maintaining temperatures above a threshold inside the tumor

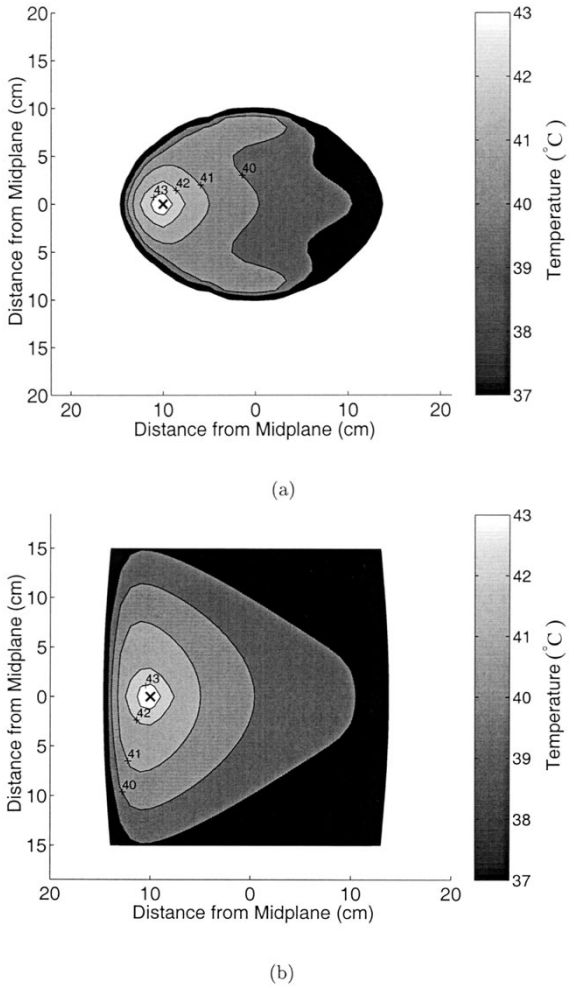

Fig. 10. Temperature field resulting from optimized driving signals for a well-perfused tumor embedded in the CDRH phantom. The center of the 2-cm-radius tumor is indicated by a cross (×) and is offset 10 cm along the major axis of the phantom. (a) Axial midplane. (b) Coronal midplane.

and below a different threshold outside the tissue has been converted into a numerical optimization problem, which can be approximately solved algorithmically. Numerical results have been presented which illustrate the ability of the technique to deal with realistic inhomogeneities and computationally burdensome models.

The method as described can be used to find a good set of array driving parameters for a patient-specific model ("prospective" dosimetry) as part of a treatment planning procedure. Additionally, various applicators can be simulated on the same patient model ("comparative" dosimetry) in order to evaluate the merits of each in a quantitative way. It has been shown that the method can easily accommodate alternative thermal models to the BHTE, as well as alternative numerical modeling and optimization techniques. It is the hope of the authors that development of the next generation of electromagnetic APAs will be eased by methods such as the one presented herein.

ACKNOWLEDGMENT

The authors would like to thank Prof. A. Webb, University of Illinois at Urbana-Champaign, for stimulating their interest in electromagnetic hyperthermia. Additionally, thanks go to Dr. I. G. Zubal, Yale School of Medicine, New Haven, CT, for generously providing the anatomically realistic data used in this paper. D. Lambalot, Compaq Computer Corporation, Marlboro, MA, for providing considerable computational assistance in generating the three-dimensional results. The careful reading of the manuscript by an anonymous reviewer has enhanced this paper's accuracy and clarity.

REFERENCES

[1] J. Overgaard, D. Gonzalez, M. Hulshof, G. Arcangeli, O. Dahl, O. Mella, and S. Bentzen, "Randomized trial of hyperthermia as an adjuvant to radiotherapy for recurrent or metastatic malignant melanoma," *Lancet*, vol. 345, pp. 540–543, 1995.

[2] P. Wust, M. Seebass, J. Nadobny, P. Deuflhard, G. Monich, and R. Felix, "Simulation studies promote technological development of radio-frequency phased array hyperthermia," *Int. J. Hyperthermia*, vol. 12, no. 4, pp. 477–494, 1996.

[3] P. F. Turner, "Regional hyperthermia with an annular phased array," *IEEE Trans. Biomed. Eng.*, vol. BME-31, pp. 106–114, Jan. 1984.

[4] P. Wust, J. Nadobny, R. Felix, P. Deuflhard, A. Louis, and W. John, "Strategies for optimized application of annular-phased-array systems in clinical hyperthermia," *Int. J. Hyperthermia*, vol. 7, no. 1, pp. 157–173, 1991.

[5] D. M. Sullivan, "Mathematical methods for treatment planning in deep regional hyperthermia," *IEEE Trans. Microwave Theory Tech.*, vol. 39, pp. 864–872, May 1991.

[6] B. J. James and D. M. Sullivan, "Creation of three-dimensional patient models for hyperthermia treatment planning," *IEEE Trans. Biomed. Eng.*, vol. 39, pp. 238–242, Mar. 1992.

[7] ——, "Direct use of CT scans for hyperthermia treatment planning," *IEEE Trans. Biomed. Eng.*, vol. 39, pp. 845–851, Aug. 1992.

[8] F. Bardati, A. Borrani, A. Gerardino, and G. A. Lovisolo, "SAR optimization in a phased array radiofrequency hyperthermia system," *IEEE Trans. Biomed. Eng.*, vol. 42, pp. 1201–1207, Dec. 1995.

[9] K. S. Nikita, N. G. Maratos, and N. K. Uzunoglu, "Optimization of the deposited power distribution inside a layered lossy medium irradiated by a coupled system of concentrically placed waveguide applicators," *IEEE Trans. Biomed. Eng.*, vol. 45, pp. 909–920, July 1998.

[10] K. D. Paulsen, S. Geimer, J. Tang, and W. E. Boyse, "Optimization of pelvic heating rate distributions with electromagnetic phased arrays," *Int. J. Hyperthermia*, vol. 15, no. 3, pp. 157–186, 1999.

[11] M. Knudsen and U. Hartmann, "Optimal temperature control with a phased array hyperthermia system," *IEEE Trans. Microwave Theory Tech.*, vol. 34, pp. 597–603, May 1986.

[12] P. VanBaren and E. S. Ebbini, "Multipoint temperature control during hyperthermia treatments: Theory and simulation," *IEEE Trans. Biomed. Eng.*, vol. 42, pp. 818–827, Aug. 1995.

[13] E. Hutchinson, M. Dahleh, and K. Hynynen, "The feasibility of MRI feedback control for intracavity phased array hyperthermia treatments," *Int. J. Hyperthermia*, vol. 14, no. 1, pp. 39–56, 1998.

[14] K. S. Nikita, N. G. Maratos, and N. K. Uzunoglu, "Optimal steady-state temperature distribution for a phased array hyperthermia system," *IEEE Trans. Biomed. Eng.*, vol. 40, pp. 1299–1306, Dec. 1993.

[15] S. K. Das, S. T. Clegg, and T. V. Samulski, "Computational techniques for fast hyperthermia temperature optimization," *Med. Phys.*, vol. 26, no. 2, pp. 319–328, Feb. 1999.

[16] J. Lang, B. Erdmann, and M. Seebass, "Impact of nonlinear heat transfer on temperature control in regional hyperthermia," *IEEE Trans. Biomed. Eng.*, vol. 46, pp. 1129–1138, Sept. 1999.

[17] K. S. Yee, "Numerical solution of initial boundary value problems involving Maxwell's equations in isotropic media," *IEEE Trans. Antennas Propagat.*, vol. AP-14, pp. 302–307, Mar. 1966.

[18] C.-Q. Wang and O. P. Gandhi, "Numerical simulation of annular phased arrays for anatomically based models using the FDTD method," *IEEE Trans. Microwave Theory Tech.*, vol. 37, pp. 118–126, Jan. 1989.

[19] D. M. Sullivan, "Three-dimensional computer simulation in deep regional hyperthermia using the finite-difference time-domain method," *IEEE Trans. Microwave Theory Tech.*, vol. 38, Feb. 1990.

[20] J.-Y. Chen and O. P. Gandhi, "Numerical simulation of annular-phased arrays of dipoles for hyperthermia of deep-seated tumors," *IEEE Trans. Biomed. Eng.*, vol. 39, pp. 209–216, Mar. 1992.

[21] P. C. Cherry and M. F. Iskander, "FDTD analysis of power deposition patterns of an array of interstitial antennas for use in microwave hyperthermia," *IEEE Trans. Microwave Theory Tech.*, vol. 40, pp. 1692–1700, Aug. 1992.
[22] D. M. Sullivan, D. Buechler, and F. A. Gibbs, "Comparison of measured and simulated data in an annular phased array using an inhomogeneous phantom," *IEEE Trans. Microwave Theory Tech.*, vol. 40, pp. 600–604, Mar. 1992.
[23] C. E. Reuter, A. Taflove, V. Sathiaseelan, M. Piket-May, and B. B. Mittal, "Unexpected physical phenomena indicated by FDTD modeling of the Sigma-60 deep hyperthermia applicator," *IEEE Trans. Microwave Theory Tech.*, vol. 46, pp. 313–319, Apr. 1998.
[24] H. H. Pennes, "Analysis of tissue and arterial blood temperatures in the resting human arm," *J. Appl. Physiol.*, vol. 1, pp. 93–122, 1948.
[25] P.-Y. Cresson, C. Michel, L. Dubois, M. Chive, and J. Pribetich, "Complete three-dimensional modeling of new microstrip–microslot applicators for microwave hyperthermia using the FDTD method," *IEEE Trans. Microwave Theory Tech.*, vol. 42, pp. 2657–2666, Dec. 1994.
[26] J.-C. Camart, D. Despretz, M. Chive, and J. Pribetich, "Modeling of various kinds of applicators used for microwave hyperthermia based on the FDTD method," *IEEE Trans. Microwave Theory Tech.*, vol. 44, pp. 1811–1818, Oct. 1996.
[27] D. G. Luenberger, *Introduction to Linear and Nonlinear Programming*. Reading, MA: Addison-Wesley, 1973.
[28] A. Jennings and J. J. McKeown, *Matrix Computation*, 2nd ed. New York: Wiley, 1992.
[29] C. Johnson, R. Kress, R. Roemer, and K. Hynynen, "Multi-point feedback control system for scanned, focused ultrasound hyperthermia," *Phys. Med. Biol.*, vol. 35, no. 6, pp. 781–786, 1990.
[30] I. G. Zubal, C. R. Harrell, E. O. Smith, Z. Rattner, G. Gindi, and P. B. Hoffer, "Computerized three-dimensional segmented human anatomy," *Med. Phys.*, vol. 21, no. 2, pp. 299–302, Feb. 1992.
[31] J. P. Berenger, "A perfectly matched layer for the absorption of electromagnetic waves," *J. Comput. Phys.*, vol. 114, pp. 185–200, 1994.
[32] M. E. Kowalski, "Modeling, optimization, and control of electromagnetic oncological hyperthermia," M.S. thesis, Dept. Elect. Comput. Eng., Univ. Illinois at Urbana-Champaign, Urbana, IL, 1999.
[33] C. Gabriel, S. Gabriel, and E. Corthout, "The dielectric properties of biological tissues: I. Literature survey," *Phys. Med. Biol.*, vol. 41, pp. 2231–2249, 1996.
[34] S. Gabriel, R. W. Lau, and C. Gabriel, "The dielectric properties of biological tissues: III. Parametric models for the dielectric spectrum of tissues," *Phys. Med. Biol.*, vol. 41, pp. 2271–2293, 1996.
[35] F. A. Duck, *Physical Properties of Tissue: A Comprehensive Reference*. New York: Academic, 1990.

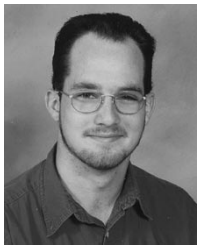

Marc E. Kowalski (S'95–M'97) was born on September 29, 1975, in Neptune, NJ. He received the B.S.E.E. degree from the New Jersey Institute of Technology, Newark, NJ, in 1997, the M.S. degree from the University of Illinois at Urbana-Champaign, in 1999, and is currently working toward the Ph.D. degree in electrical engineering at the University of Illinois at Urbana-Champaign.

His current research interests are in the applications of computational science and systems theory to biomedical problems.

Mr. Kowalski is a student member of the Society for Industrial and Applied Mathematics (SIAM) and the International Society for Magnetic Resonance in Medicine (ISMRM). He is an associate member of Sigma Xi. He has served as a technical reviewer for the IEEE TRANSACTIONS ON BIOMEDICAL ENGINEERING and the IEEE TRANSACTIONS ON ANTENNAS AND PROPAGATION. He was a recipient of the National Science Foundation Graduate Fellowship and the IEEE Microwave Theory and Techniques Society (IEEE MTT-S) Graduate Fellowship.

Jian-Ming Jin (S'87–M'89–SM'94) received the B.S. and M.S. degrees in applied physics from Nanjing University, Nanjing, China, in 1982 and 1984, respectively, and the Ph.D. degree in electrical engineering from The University of Michigan at Ann Arbor, in 1989.

He is currently an Associate Professor of electrical and computer engineering and Associate Director of the Center for Computational Electromagnetics at the University of Illinois at Urbana-Champaign. He has authored or co-authored over 90 papers in refereed journals and several book chapters. He has also authored *The Finite Element Method in Electromagnetics* (New York: Wiley, 1993) and *Electromagnetic Analysis and Design in Magnetic Resonance Imaging* (Boca Raton, FL: CRC Press, 1998), and co-authored *Computation of Special Functions* (New York: Wiley, 1996). His current research interests include computational electromagnetics, scattering and antenna analysis, electromagnetic compatibility, and magnetic resonance imaging. His is often listed in the University of Illinois at Urbana-Champaign's List of Excellent Instructors. He currently serves as an Associate Editor of *Radio Science* and is also on the Editorial Board for *Electromagnetics Journal* and *Microwave and Optical Technology Letters*.

Dr. Jin is a member of Commission B of USNC/URSI, Tau Beta Pi, and the International Society for Magnetic Resonance in Medicine. He served as an associate editor for the IEEE TRANSACTIONS ON ANTENNAS AND PROPAGATION (1996–1998). He was the Symposium co-chairman and technical program chairman of the Annual Review of Progress in Applied Computational Electromagnetics in 1997 and 1998, respectively. He was a recipient of the 1994 National Science Foundation Young Investigator Award and the 1995 Office of Naval Research Young Investigator Award. He also received a 1997 Xerox Research Award presented by the College of Engineering, University of Illinois at Urbana-Champaign, and was appointed the first Henry Magnuski Outstanding Young Scholar in the Department of Electrical and Computer Engineering in 1998.